CHEMISTRY
A EUROPEAN JOURNAL

DOI: 10.1002/chem.201001040

Slow Magnetic Relaxation from Hard-Axis Metal Ions in Tetranuclear Single-Molecule Magnets

Erik Tancini,[a] Maria Jesus Rodriguez-Douton,[a] Lorenzo Sorace,[b] Anne-Laure Barra,[c] Roberta Sessoli,[b] and Andrea Cornia*[a]

Abstract: We report the synthesis of the novel heterometallic complex $[Fe_3Cr(L)_2(dpm)_6]\cdot Et_2O$ (**Fe_3CrPh**) (Hdpm = dipivaloylmethane, H_3L = 2-hydroxymethyl-2-phenylpropane-1,3-diol), obtained by replacing the central iron(III) atom by a chromium(III) ion in an Fe_4 propeller-like single-molecule magnet (SMM). Structural and analytical data, high-frequency EPR (HF-EPR) and magnetic studies indicate that the compound is a solid solution of chromium-centred Fe_3Cr ($S=6$) and Fe_4 ($S=5$) species in an 84:16 ratio. Although SMM behaviour is retained, the $|D|$ parameter is considerably reduced as compared with the corresponding tetra-iron(III) propeller ($D=-0.179$ vs. $-0.418\ cm^{-1}$), and results in a lower energy barrier for magnetisation reversal ($U_{eff}/k_B=7.0$ vs. 15.6 K). The origin of magnetic anisotropy in **Fe_3CrPh** has been fully elucidated by preparing its Cr- and Fe-doped Ga_4 analogues, which contain chromium(III) in the central position (c) and iron(III) in two magnetically distinct peripheral sites (p1 and p2). According to HF-EPR spectra, the Cr and Fe dopants have hard-axis anisotropies with $D_c=0.470(5)\ cm^{-1}$, $E_c=0.029(1)\ cm^{-1}$, $D_{p1}=0.710(5)\ cm^{-1}$, $E_{p1}=0.077(3)\ cm^{-1}$, $D_{p2}=0.602(5)\ cm^{-1}$, and $E_{p2}=0.101(3)\ cm^{-1}$. Inspection of projection coefficients shows that contributions from dipolar interactions and from the central chromium(III) ion cancel out almost exactly. As a consequence, the easy-axis anisotropy of **Fe_3CrPh** is entirely due to the peripheral, hard-axis-type iron(III) ions, the anisotropy tensors of which are necessarily orthogonal to the threefold molecular axis. A similar contribution from peripheral ions is expected to rule the magnetic anisotropy in the tetra-iron(III) complexes currently under investigation in the field of molecular spintronics.

Keywords: chromium · EPR spectroscopy · iron · magnetic properties · single-molecule magnets

Introduction

Large metal-ion clusters behaving as single molecule magnets (SMMs) have been the target of undiminished interest in the last 15 years. As common features, these molecules display a giant spin and a large Ising-type magnetic anisotropy in their ground state. For this reason, many SMMs known to date comprise arrays of easy-axis paramagnetic ions, such as high-spin manganese(III). Furthermore, the molecular structure is such that the easy axes of individual ions are approximately collinear with each other, so as to contribute constructively to the molecular anisotropy.[1]

Although new classes of SMMs are usually obtained by serendipitous assembly, much work is now devoted to the controlled engineering of known structural types in order to improve their performances and/or to introduce additional functionalities.[2] Alteration of the magnetic core of SMMs with the insertion of different metal ions at specific sites is of great interest as a route for the enhancement of magnetic properties and clarification of the origin of magnetic anisotropy. On the other hand, functionalisation of SMMs is crucial if SMMs have to be incorporated into devices or deposited on surfaces for applications in the field of molecular spintronics.[3]

[a] E. Tancini, Dr. M. J. Rodriguez-Douton, Prof. Dr. A. Cornia
Department of Chemistry & INSTM research unit
University of Modena and Reggio Emilia
Via G. Campi 183, 41100 Modena (Italy)
Fax: (+39) 059-373543
E-mail: acornia@unimore.it

[b] Dr. L. Sorace, Prof. Dr. R. Sessoli
Department of Chemistry "Ugo Schiff" & INSTM research unit
University of Florence
Via della Lastruccia 3-13, 50019 Sesto Fiorentino (FI) (Italy)

[c] Dr. A.-L. Barra
Laboratoire National des Champs Magnétiques Intenses—CNRS
BP 166, 25 Avenue des Martyrs, 38042 Grenoble Cedex 9 (France)

Supporting information for this article is available on the WWW under http://dx.doi.org/10.1002/chem.201001040.

A unique combination of structural and electronic robustness and ease of functionalisation has been recently found in a family of tetra-iron(III) SMMs with a propeller-like structure and an $S=5$ ground state (Scheme 1a). Function-

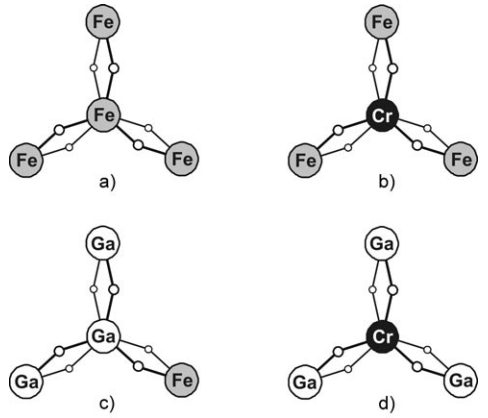

Scheme 1. Sketched structure of the O-bridged metal core in a) **Fe_4Ph**, b) **Fe_3CrPh**, c) **(Ga,Fe)$_4$Ph**, and d) **(Ga,Cr)$_4$Ph**.

alised complexes of this class have been prepared, which can be deposited on surfaces,[4,5] or even thermally evaporated,[6] without structural disruption, as demonstrated by the retention of SMM behaviour. Heterometallic Fe–Cr and Fe–Al propeller-like complexes were also assembled by Saalfrank and co-workers using *N*-methyldiethanolamine ligands,[7] but their physical properties were not reported, and the possibility of metal scrambling was not discussed.

In this paper, we report the controlled assembly of a heterometallic Fe–Cr SMM, $[Fe_3Cr(L)_2(dpm)_6]\cdot Et_2O$ (**Fe_3CrPh**), which is found to be isomorphous with the corresponding tetra-iron(III) compound (**Fe_4Ph**), and features chromium(III) as the central metal ion (Scheme 1b). The ligand H_3L=2-hydroxymethyl-2-phenylpropane-1,3-diol was chosen because phenyl-substituted tripods usually afford crystalline complexes in high yield.[6,8,9] The complex has an $S=6$ ground state with an easy-axis anisotropy and exhibits SMM properties. To disclose the origin of magnetic anisotropy in **Fe_3CrPh** and in the structurally related class of tetra-iron(III) propellers, an isomorphous tetragallium(III) cluster, $[Ga_4(L)_2(dpm)_6]\cdot Et_2O$ (**Ga_4Ph**), was prepared, and its Fe- and Cr-doped variants (Scheme 1c,d) were studied by electronic spectroscopy and high-frequency EPR (HF-EPR). As a firm experimental confirmation of previous inductions based on magnetostructural correlations,[8,10] the iron(III) and chromium(III) ions in the structures have a hard-axis anisotropy. A large non-collinearity of anisotropy tensors is proposed to explain SMM behaviour in the presence of hard-axis metal ions.

Results and Discussion

Synthesis: A large variety of tetra-iron(III) propellers were previously assembled by the reaction route described in Equations (1)–(3) with $M=M'=Fe^{3+}$.[8,10] According to this procedure, compound $[Fe_4(OMe)_6(dpm)_6]$ (**Fe_4**) is first prepared from the dimeric precursor $[Fe_2(OMe)_2(dpm)_4]$ (**Fe_2**) [Eqs. (1) and (2)]; it is then reacted with tripodal ligands (H_3L) derived from 2-(hydroxymethyl)propane-1,3-diol to afford the desired products in pure, crystalline form and in good to excellent yield [Eq. (3)].

$$2\,MCl_3 + 4\,Hdpm + 6\,NaOMe \rightarrow [M_2(OMe)_2(dpm)_4] + 4\,MeOH + 6\,NaCl \quad (1)$$

$$3\,[M_2(OMe)_2(dpm)_4] + 2\,M'Cl_3 + 6\,NaOMe \rightarrow 2\,[M_3M'(OMe)_6(dpm)_6] + 6\,NaCl \quad (2)$$

$$[M_3M'(OMe)_6(dpm)_6] + 2\,H_3L \rightarrow [M_3M'(L)_2(dpm)_6] + 6\,MeOH \quad (3)$$

The same procedure was tested for the preparation of mixed Fe–Cr propellers, by using $M=Fe^{3+}$ and $M'=Cr^{3+}$ (due to the polymeric nature of $CrCl_3$ and to the inertness of the chromium(III) ion, $CrCl_3$ must be first converted to monomeric $[CrCl_3(thf)_3]$[11]). Though the synthesis afforded reddish-brown crystals of $[Fe_3Cr(OMe)_6(dpm)_6]$ (**Fe_3Cr**) in good yield (80%), the Fe:Cr atomic ratio determined by complexometric titration[12] was found to be 4.1–5.2, quite different from that actually used in the synthesis (3.0).[13] In fact, the magnetic properties, with a $\chi_m T$ value approaching 18.2 emu K mol^{-1} at low temperature, suggest the presence of a large fraction of homometallic species in the crystals and/or extensive metal scrambling (see Supporting Information).

We thus preferred not to use **Fe_3Cr** in the ligand exchange reaction with tripodal ligands [Eq. (3)], and we attempted a one-pot self-assembly reaction described by Equation (4) with $M=Fe^{3+}$ and $M'=Cr^{3+}$. Using H_3L=2-(hydroxymethyl)-2-phenylpropane-1,3-diol we obtained the derivative **Fe_3CrPh** in moderate yield (54%), and the Fe:Cr atomic ratio was found to be in the range 3.8–4.1, hence smaller than in **Fe_3Cr**.[13] If the compound is taken as a solid solution of chromium-centred Fe_3Cr and Fe_4, as suggested by magnetic measurements and HF-EPR spectra (vide infra), elemental analysis indicates that the crystal comprises $\approx$84% Fe_3Cr and 16% Fe_4.

$$3\,[M_2(OMe)_2(dpm)_4] + 2\,M'Cl_3 + 6\,NaOMe + 4\,H_3L \rightarrow 2\,[M_3M'(L)_2(dpm)_6] + 6\,NaCl + 12\,MeOH \quad (4)$$

The same synthetic technique was used to prepare off-white $[Ga_4(L)_2(dpm)_6]\cdot Et_2O$ (**Ga_4Ph**) as a diamagnetic analogue of **Fe_3CrPh** and **Fe_4Ph** following Equations (1) and (4) with $M=M'=Ga^{3+}$. Furthermore, by using $M'=Ga^{3+}/Fe^{3+}$

(3:1) or $M' = Ga^{3+}/Cr^{3+}$ (3:1) in Equation (4) we obtained the Fe- and Cr-doped derivatives, **$(Ga,Fe)_4$Ph** and **$(Ga,Cr)_4$Ph**, as yellow and blue crystals, respectively.

X-ray structures: **Fe_3CrPh** is isomorphous to the corresponding homometallic compound and crystallises in the monoclinic space group *C*2/*c*, with four cluster molecules and four diethyl ether molecules per unit cell. Selected crystal data and refinement and structural parameters can be found in the Supporting Information. The molecular structure as determined through single-crystal X-ray diffraction at 120 K is shown in Figure 1, and Figure 2 provides a view of the

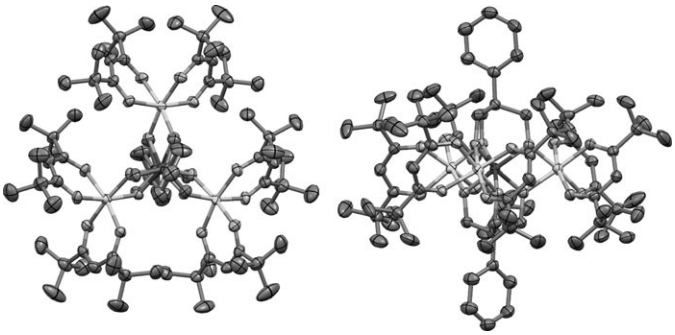

Figure 1. Molecular structure of **Fe_3CrPh** viewed perpendicular to the metal plane (left) and parallel to it (right). Thermal ellipsoids are drawn at 50% probability. Hydrogen atoms and the lattice diethyl ether molecule are omitted.

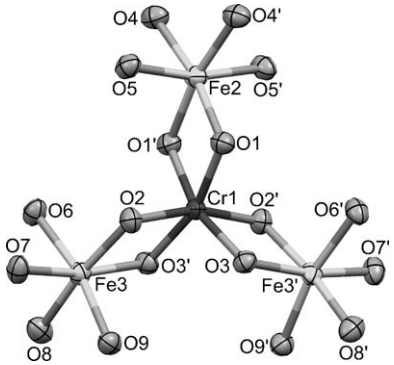

Figure 2. Metal–oxygen core of **Fe_3CrPh** with the atom labelling scheme. Thermal ellipsoids are drawn at 50% probability.

metal–oxygen core. The tetrametallic moiety shows no relevant disorder effects, except for a *t*Bu group that is disordered over two positions with 74 and 26% occupancy, respectively. In spite of the close atomic numbers of Cr ($Z = 24$) and Fe ($Z = 26$), a hint at preferential occupation of the central position by Cr rather than by Fe was obtained from the analysis of best-fit displacement parameters.

Selected geometrical parameters for **Fe_3CrPh** are gathered in Table 1 along with the corresponding values for the homometallic complex **Fe_4Ph**. In accordance with the labelling scheme of Figure 2, M1 labels the central metal, M2 is used to indicate the peripheral metal lying on the twofold symmetry axis, and M3 labels the remaining metal site in general position. Note that the three peripheral ions, though chemically equivalent, are found in two crystallographically distinct sites in a 1:2 ratio. The M1–O distances range from 1.958 to 1.967 Å in **Fe_3CrPh**, whereas in **Fe_4Ph** they are found between 1.965 and 1.981 Å. It is seen that corresponding M1–O distances are invariably smaller in **Fe_3CrPh**, whereas the M2–O and M3–O separations are larger or equal within experimental error to those observed in the homometallic derivative (observed ranges: 1.977–2.031 Å in **Fe_3CrPh** and 1.972–2.032 Å in **Fe_4Ph**). Moreover, a meaningful comparison can be made with the two dimeric complexes **Fe_2**[14] and $[Cr_2(OMe)_2(dpm)_4]$ (**Cr_2**),[15] which contain the same coordination environment for the metal ions as in the peripheral sites of the tetranuclear species. The M–O distances in the above-mentioned dimers are in the range 1.965(5)–2.013(6) Å for M = Fe and 1.945(3)–1.975(3) Å for M = Cr, and provide a strong indication that the peripheral metal sites in **Fe_3CrPh** are predominantly occupied by Fe. The intermetal separations M1···M2 and M1···M3 are also different, being 3.0472(6), 3.0406(4) Å in **Fe_3CrPh** and 3.0780(8), 3.0726(6) Å in **Fe_4Ph**. The following features are also evident:

1) The smaller distortion by trigonal rotation that affects the coordination sphere of the central metal ion in **Fe_3CrPh** (see Supporting Information and reference [10]).

Table 1. Comparison between selected distances and angles in **Fe_4Ph** and **Fe_3CrPh** with estimated standard deviations in parentheses.[a]

	Fe_4Ph	**Fe_3CrPh**		**Fe_4Ph**	**Fe_3CrPh**
M1···M2	3.0780(8)	3.0472(6)	M1···M3	3.0726(6)	3.0406(4)
M2···M3	5.2925(7)	5.2461(5)	M3···M3′	5.3880(11)	5.3175(6)
M1–O1	1.9801(19)	1.9654(14)	M1–O2	1.9650(18)	1.9578(14)
M1–O3	1.9813(19)	1.9670(14)	M2–O1	1.9718(19)	1.9843(14)
M2–O4	1.995(2)	2.0025(15)	M2–O5	2.0321(19)	2.0309(14)
M3–O2	1.9784(19)	1.9892(14)	M3–O3′	1.9718(18)	1.9771(14)
M3–O6	1.9853(19)	1.9899(14)	M3–O7	2.004(2)	2.0105(15)
M3–O8	1.993(2)	2.0006(15)	M3–O9	1.9909(19)	1.9963(14)
M2···M1···M3	118.74(1)	119.02(1)	M3···M1···M3′	122.51(2)	121.95(2)
O1-M1-O2	88.63(8)	89.42(6)	O1-M1-O3	89.16(8)	89.94(6)
O1-M1-O1′	77.49(11)	79.47(8)	O2-M1-O3′	77.84(8)	79.67(6)
O2-M1-O3	89.94(8)	90.59(6)	O2-M1-O2′	159.02(11)	164.35(9)
O2-M1-O1′	107.93(8)	102.68(6)	O1′-M1-O3	157.17(8)	162.82(6)
O3-M1-O3′	108.90(11)	103.29(8)	O1-M2-O1′	77.88(11)	78.57(8)
O1-M2-O4	167.45(8)	169.68(6)	O1′-M2-O4	95.31(8)	94.71(6)
O4-M2-O4′	93.22(12)	92.96(9)	O1-M2-O5	86.44(8)	88.39(6)
O1-M2-O5′	103.12(8)	101.39(6)	O4-M2-O5	84.86(8)	85.24(6)
O4′-M2-O5	86.79(8)	86.11(6)	O5-M2-O5′	167.83(11)	167.44(8)
O2-M3-O3′	77.75(8)	78.68(6)	O2-M3-O6	99.44(9)	97.15(6)
O3′-M3-O6	88.85(8)	91.22(6)	O3′-M3-O9	100.03(8)	98.04(6)
O2-M3-O9	89.66(8)	91.95(6)	O6-M3-O9	168.50(8)	168.13(6)
O3′-M3-O8	94.10(9)	93.60(6)	O2-M3-O8	169.54(9)	171.61(6)
O6-M3-O8	86.81(9)	86.18(6)	O9-M3-O8	85.29(8)	85.85(6)
O3′-M3-O7	166.88(8)	168.69(6)	O2-M3-O7	91.27(8)	90.71(6)
O6-M3-O7	85.88(8)	86.21(6)	O9-M3-O7	86.89(8)	86.08(6)
O8-M3-O7	97.59(9)	97.20(6)	M2-O1-M1	102.31(9)	100.98(7)
M3-O2-M1	102.37(8)	100.77(6)	M3-O3′-M1	102.02(8)	100.87(6)

[a] Primed atoms are related to unprimed ones by a twofold rotation around M1···M2.

2) The smaller value of the "helical pitch", which describes the tilting of the $M1(O)_2M2$ and $M1(O)_2M3$ moieties with respect to the metal ion plane (64.4 vs. 68.8°) (see Supporting Information and reference [10]).
3) The smaller angles at the bridging oxygen atoms (average: 100.9° vs. 102.2°).

The same trend emerges by comparing the structures of **Fe_3Cr** and **Fe_4** (see Supporting Information). Altogether, these differences suggest that the ionic radius of the central metal ion is smaller in **Fe_3CrPh** than in **Fe_4Ph**. According to Shannon and Prewitt, the ionic radius of chromium(III) (0.62 Å) is indeed smaller than that of high-spin iron(III) (0.65 Å).[16] The preferential occupation of the central site by chromium(III) (Scheme 1b) is fully supported by the magnetic studies reported in the next section, and may be a consequence of both thermodynamic and kinetic effects; we simply notice here that the chemical inertness of chromium(III) complexes is expected to result in exceeding kinetic stability for the $[Cr(L)_2]^{3-}$ unit, which comprises two tridentate ligands facially bound to the same metal ion. As a final remark, combined elemental analysis and magnetic data indicate that the lattice comprises ≈84% of chromium-centred Fe_3Cr and 16% of Fe_4 species (see below), so that the observed bond lengths and other geometrical parameters are weighted average values.

Ga_4Ph is isomorphous with **Fe_3CrPh** and **Fe_4Ph** (see Supporting Information for details). The observed structural differences are consequence of the smaller ionic radius of gallium(III) (0.62 Å) with respect to high-spin iron(III) (0.65 Å).[16] The Ga1–O distances are in the range 1.937–1.952 Å, and Ga2–O and Ga3–O range from 1.933 to 1.982 Å. The intermetal separations Ga1···Ga2 and Ga1···Ga3 are 3.0072(5) and 3.0012(3) Å, respectively. The distortion by trigonal rotation of Ga1 is comparable to that found in **Fe_3CrPh**. However, slight trigonal compression leads to a smaller helical pitch (63.8 vs. 64.4°).

Direct current magnetic studies: Microcrystalline samples of **Fe_3Cr** and **Fe_3CrPh** were investigated by direct current (dc) magnetometry by measuring the temperature dependence of the molar magnetic susceptibility (χ_m) in low fields (1–10 kOe). Magnetic data for **Fe_3Cr** are reported in the Supporting Information and suggest significant metal scrambling. The χ_mT versus T plot for **Fe_3CrPh**, displayed in Figure 3, suggests the presence of antiferromagnetic interactions, which are responsible for the decrease of χ_mT when cooling down from room temperature. However, the rapid increase of the χ_mT value below 100 K is indicative of a high-spin ground state. The highest χ_mT value observed, 19.3 emu K mol^{-1}, is larger than expected for Fe_4 ($S=5$, 15.0 emu K mol^{-1}) and iron-centred Fe_3Cr species ($S=4$, 10.0 emu K mol^{-1}), being indeed close to the Curie constant for an $S=6$ state (21.0 emu K mol^{-1} for $g=2.00$). The low-temperature magnetism of the compound is thus a clear indication that the chromium ion is preferentially incorporated as the central ion. A quantitative analysis of the χ_mT versus T curve was based on a Heisenberg spin-Hamiltonian to account for nearest neighbour (J) and next-nearest neighbour (J') interactions, assuming threefold symmetry and using the $J\mathbf{S}_i\cdot\mathbf{S}_j$ convention.[17] In a first treatment (**I**), a chromium-centred Fe_3Cr model was used. In a second approach (**II**), a mixture of chromium-centred Fe_3Cr and Fe_4 species was assumed (84:16), in accordance with the results of elemental analysis; the experimental data were corrected for the contribution of Fe_4, evaluated on the basis of the susceptibility values already available.[8] The best-fit parameters so obtained are: **I**: $J=11.38(11)$ cm^{-1}, $J'=-0.62(4)$ cm^{-1}, $g=1.938(2)$, $\theta=-0.135(8)$ K; **II**: $J=12.52(7)$ cm^{-1}, $J'=-0.25(2)$ cm^{-1}, $g=1.9744(13)$, $\theta=-0.110(5)$ K (θ is a Curie–Weiss temperature used to account for the drop of χ_mT at the lowest temperatures). Besides providing a better fit to the experimental data, model **II** is preferable as it affords a g factor closer to 2.00, as expected for metal ions with an orbitally non-degenerate ground state. With these values of the coupling constants, the first excited states are a couple of degenerate $S=5$ states at 20.7 cm^{-1} from the ground $S=6$ multiplet. Magnetisation isotherms at 1.9, 2.5 and 4.5 K, measured as a function of applied field, are included in the inset of Figure 3. The saturation magnetisation is close to $12N_A\mu_B$, which is the expected value for an $S=6$ state with $g=2.000$. Data analysis was performed using a spin-Hamiltonian for an isolated $S=6$ spin with second-order axial anisotropy described by the zero-field splitting (zfs) D parameter.[17] Again, two distinct approaches were followed: **I**) direct fitting of experimental data with the $S=6$ model, hence neglecting species other than chromium-centred Fe_3Cr; **II**) fitting of corrected data, obtained by subtracting the contribution of Fe_4, as in the treatment of susceptibility measurements. The best-fit parameters so obtained are: **I**: $D=-0.186(2)$ cm^{-1} and $g=1.932(2)$; **II**: $D=-0.175(3)$ cm^{-1} and $g=1.988(3)$. Again, model **II** is superior as far as the g value is concerned. Note that with both models an accurate fitting was not possible imposing a positive D parameter. In

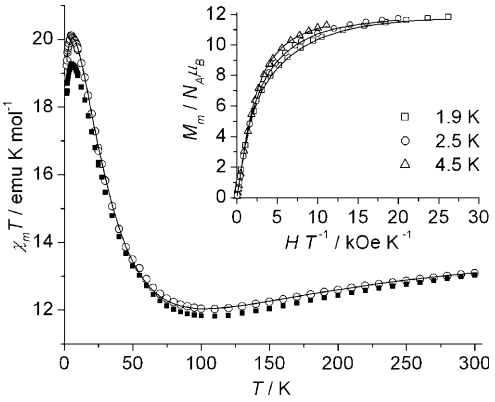

Figure 3. Magnetic properties of **Fe_3CrPh** measured in dc mode. The main panel displays raw χ_mT versus T data (■) and data corrected for the presence of a 16% molar fraction of **Fe_4Ph** (○). The inset shows M_m versus H/T data, corrected as above, at three temperatures. The solid lines represent best-fit simulated data with model **II**, as described in the main text.

summary, dc magnetic studies strongly support the occurrence of chromium-centred Fe_3Cr as the dominant species in the lattice of **Fe_3CrPh**.

Electronic spectra in solution: Compound **Fe_3CrPh** is black–red in the solid state, whereas **Fe_4Ph** is red–orange. Solutions of the two complexes in toluene at mM concentration are dark reddish–brown and yellow–orange, respectively, and their UV/Vis absorption spectra are shown in Figure 4.

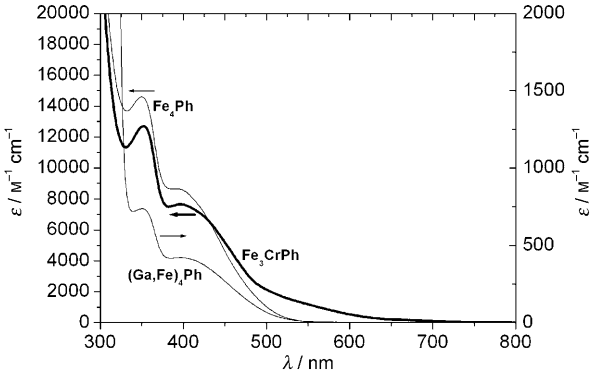

Figure 4. UV/Vis absorption spectra of **Fe_4Ph** (0.60 mM, optical path 0.1 cm), **(Ga,Fe)$_4$Ph** (3.9 mM, optical path 0.5 cm), and **Fe_3CrPh** (0.66 mM, optical path 0.1 cm) in toluene.

In the region from 330 to 800 nm **Fe_4Ph** is characterised by strong absorptions at 350 and 395 nm, corresponding to the $t_{2g}\rightarrow\pi^*$ and $\pi\rightarrow e_g$ charge transfer (CT) transitions of iron(III) β-diketonate complexes.[18a] Very similar bands are found in **Fe_3CrPh** (352 and 396 nm), in agreement with the occurrence of iron(III) in the peripheral metal sites. In addition, **Fe_3CrPh** features a broad shoulder around 520–540 nm, which is not detected in **Fe_4Ph** and has an $\varepsilon_{max}\cong 1200\,M^{-1}cm^{-1}$ (from spectra deconvolution). Although the band position (19200–18500 cm^{-1}) is not far from the $^4A_{2g}\rightarrow{}^4T_{2g}$ transition energy (=10 Dq) of octahedral chromium(III) complexes with oxygen ligands (for example, 17400 cm^{-1} in $[Cr(H_2O)_6]^{3+}$ and $[Cr(OMe)_3]$, 17700 cm^{-1} in $[Cr(dpm)_3]$), the band intensity is one order of magnitude larger than expected.[18b] The origin of such a band will be discussed after presentation of the spectra of **(Ga,Fe)$_4$Ph** and **(Ga,Cr)$_4$Ph**.

Solutions of **(Ga,Fe)$_4$Ph** in toluene at mM concentration are yellow, and their UV/Vis absorption spectrum is shown in Figure 4. The qualitative resemblance to the spectrum of **Fe_4Ph** strongly supports the hypothesis that in **(Ga,Fe)$_4$Ph** the iron(III) ion is found predominantly on peripheral metal sites (Scheme 1c).

Solutions of **(Ga,Cr)$_4$Ph** in toluene at mM concentration are blue, and their UV/Vis absorption spectrum is shown in Figure 5. In the visible region, the spectrum features a broad band at 625 nm ($\varepsilon_{max}\cong 160\,M^{-1}cm^{-1}$) assigned to the $^4A_{2g}\rightarrow{}^4T_{2g}$ transition of chromium(III) in octahedral symmetry (whence 10 Dq≅16000 cm^{-1}). Only weak absorptions are

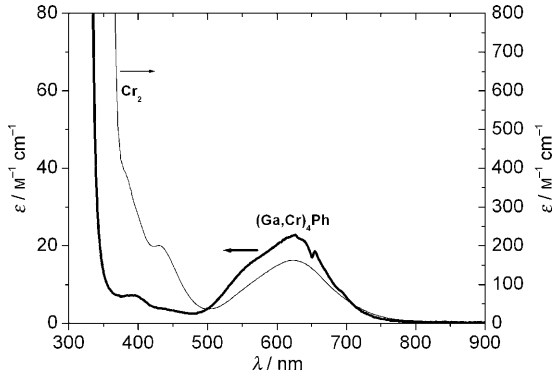

Figure 5. UV/Vis absorption spectra of **Cr_2** (4.0 mM, optical path 0.5 cm) and of **(Ga,Cr)$_4$Ph** (3.9 mM, optical path 1.0 cm) in toluene.

found between 370 and 480 nm, a region in which the $^4A_{2g}\rightarrow{}^4T_{1g}(F)$ transition is typically observed in chromium(III) complexes with oxygen ligands.[18b,c] Intense bands, probably due to CT transitions, are detected in the UV region ($\lambda<350$ nm). For comparison, Figure 5 also shows the electronic spectrum of the green dimer $[Cr_2(OMe)_2(dpm)_4]$ (**Cr_2**),[15] which contains the $(MeO)_2Cr(dpm)_2$ chromophore. Though the $^4A_{2g}\rightarrow{}^4T_{2g}$ transition is observed essentially at the same energy as in **(Ga,Cr)$_4$Ph**, the $^4A_{2g}\rightarrow{}^4T_{1g}(F)$ band is now clearly detected at 430 nm (23300 cm^{-1}) on the low-energy tail of the strong CT absorptions typical of chromium(III) β-diketonate complexes.[18d]

These differences in the spectra prove that the chromium(III) dopant in **(Ga,Cr)$_4$Ph** is predominantly not coordinated by dpm ligands. Thus, it necessarily sits in the central position of the cluster, where it is surrounded by six alkoxide-type oxygen donors (Scheme 1d).

The electronic spectra presented in Figure 5 also confirm that the intense band at 520–540 nm in **Fe_3CrPh** (Figure 4) has neither the position nor the intensity expected for the $^4A_{2g}\rightarrow{}^4T_{2g}$ transition of a chromium(III) ion in any of the two possible coordination environments (central and peripheral). Similar electronic bands were previously noticed in trinuclear basic acetates of chromium(III) and iron(III), and ascribed to simultaneous (Cr^{3+}, Fe^{3+}) double excitations.[19] In the series $[M_3O(MeCO_2)_6(L')_3]Cl$, with L′=py or H_2O and $M_3=Cr^{III}{}_3$, $Cr^{III}{}_2Fe^{III}$, $Cr^{III}Fe^{III}{}_2$, or $Fe^{III}{}_3$, the heterometallic species have intense absorption bands at approximately 19000 and 26000 cm^{-1}, which do not correspond to any band in the homometallic derivatives. As a result, whereas the homometallic derivatives with L′=py are grey–green ($Cr^{III}{}_3$) and olive green ($Fe^{III}{}_3$), $Cr^{III}{}_2Fe^{III}$ and $Cr^{III}Fe^{III}{}_2$ are purple–red and red–brown, respectively.[19]

^{1}H NMR spectra in solution: In metal complexes of dpm ligands, the *t*Bu protons (or deuterons in isotopically enriched samples) can be used as sensitive magnetic probes. In fact, disregarding pseudo-dipolar shifts (as appropriate for weakly anisotropic metal ions[20a]) the paramagnetic shift exhibited by *t*Bu protons measures the unpaired spin density delocalised on the ligands through Fermi contact interaction.

In the series of metal tris-chelates [M(dpm)$_3$], for instance, the chemical shift of *t*Bu protons varies considerably as a function of M. According to Douglas-Kissler and co-workers, at 295 K and in $CDCl_3$ solution the *t*Bu protons of [Fe(dpm)$_3$] and [Cr(dpm)$_3$] resonate at 12.9 and 2.5 ppm, respectively, compared to 1.2 ppm in the free ligand.[20b] This downfield shift is entirely due to the paramagnetism of the metal ion, as in the diamagnetic complex [Ga(dpm)$_3$] the *t*Bu groups are observed at 1.2 ppm in [D_6]benzene.[20c] Any intramolecular exchange interaction modifies the unpaired spin density on the metal ions, so that ^{1}H NMR spectroscopy can serve to investigate assembly or decomposition processes in solution.[8,17] Antiferromagnetic interactions, as those operative in **Fe_3CrPh** and **Fe_4Ph**, necessarily decrease the spin density at metal sites as compared with the mononuclear species [Fe(dpm)$_3$] or [Cr(dpm)$_3$]. With the assumption that the hyperfine coupling constant remains unchanged, the *t*Bu protons of dpm ligands should then exhibit chemical shifts in the range from around 12.9 to 1.2 ppm when bound to iron(III), and from about 2.5 to 1.2 ppm when bound to chromium(III). Further evidence for the location of the chromium ion in **Fe_3CrPh** was indeed obtained by recording ^{1}H NMR spectra of **Fe_3CrPh** and **Fe_4Ph** in [D_8]toluene at 303 K (Figure 6). The two complexes are completely stable

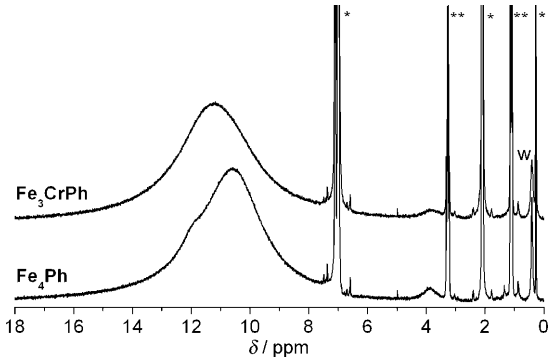

Figure 6. ^{1}H NMR spectra of **Fe_3CrPh** and **Fe_4Ph** in [D_8]toluene (8.6 and 8.2 mM, respectively) at 303 K. Narrower peaks arise from protium impurities in the solvent and silicon grease (*), from lattice diethyl ether (**) and from water traces (w).

in solution; their spectra are time independent and very different from those recorded for the diamagnetic complex **Ga_4Ph** (see Supporting Information). The *t*Bu protons of **Fe_4Ph** and **Fe_3CrPh** resonate at 10.6 and 11.2 ppm, respectively, that is, in the range expected for iron(III)-bound dpm ligands.[8] The broad peak at 3.8 ppm, observed in both compounds but not in derivatives with an alkyl substituent on the tripodal ligand, and the shoulder at 12.0 ppm in **Fe_4Ph**, are tentatively assigned to the phenyl protons of L^{3-}. The larger downfield shift observed in **Fe_3CrPh** is indicative of a higher spin density on the peripheral Fe sites. In order to check this point, we used the *J* values determined in the solid state to calculate the local *Z* component of the spins, S_{Zi}, under the conditions of the NMR experiment. The calculation, details of which can be found in the Supporting Information, showed that S_{Zi} for the peripheral metal centres is $\approx$10% larger in **Fe_3CrPh** than in **Fe_4Ph**, in agreement with the slightly larger paramagnetic shift observed in the Cr-containing species (10.0 vs. 9.4 ppm).

High-frequency EPR spectra: As compared with traditional X-band or Q-band EPR, HF-EPR provides direct information on highly anisotropic magnetic materials, including integer-spin systems, such as SMMs.[21] Furthermore, under the conditions of an HF-EPR experiment, Zeeman interaction often dominates over anisotropy energy, resulting in considerable simplification of the spectra. Finally, the transition energy (7.7 cm^{-1} at 230 GHz) can be made comparable with or larger than the thermal energy by working at liquid-helium temperature. The resulting thermal population effects provide additional information on the splitting of the spin manifolds. The 230 GHz spectra of **Fe_3CrPh** recorded at 20, 10 and 5 K are reported in Figure 7 (190 GHz spectra

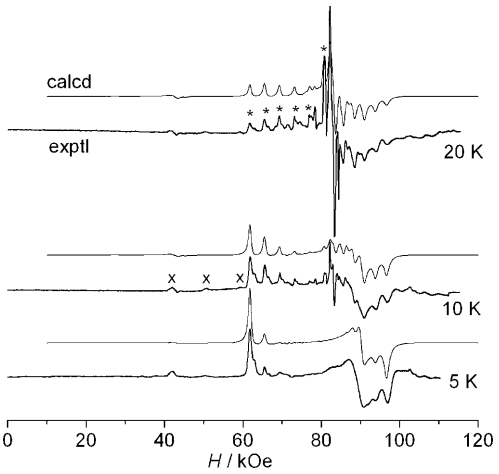

Figure 7. 230 GHz EPR spectra of **Fe_3CrPh** recorded at three different temperatures, and best-fit simulations with the parameters reported in the text. The asterisks in the 20 K spectrum mark the set of parallel transitions within the zero-field split $S=6$ state. The crosses in the 10 K spectrum highlight the weak bands attributable to **Fe_4Ph**.

can be found in Supporting Information, along with the HF-EPR characterisation of **Fe_3Cr**). In the 20 K spectrum a set of equally-spaced bands is evident between $H=61.8$ and 80.8 kOe. Such signals exhibit the maximum spectral extension with respect to the central field ($H_0=82.1$ kOe), and are thus attributable to parallel transitions of an easy-axis system.

The temperature dependence of the spectra is consistent with this hypothesis: the lowest-field signal at 61.8 kOe (which corresponds to the $|-6\rangle\rightarrow|-5\rangle$ transition) gains intensity with decreasing temperature, as expected due to preferential population of the ground $M_S=-6$ state. The line spacing, which in the high-field limit corresponds to $2|D|/(g\mu_B)$, provides $D\approx-0.18$ cm^{-1} as a rough estimate with $g=2.00$. A deeper analysis of the parallel spectral

region reveals that the band separation decreases slightly at lower fields, pointing to the presence of sizeable fourth-order axial anisotropy. Spectra were fitted using dedicated software[22a,b] based on the spin Hamiltonian shown in Equation (5), in which $\hat{\mathbf{O}}_4^0$ is the Stevens operator associated with fourth-order axial anisotropy,[22c] and the other symbols have their usual meanings.

$$\hat{\mathbf{H}}_{\mathrm{EPR}} = \mu_{\mathrm{B}}\hat{\mathbf{S}}\cdot\boldsymbol{g}\cdot\hat{\mathbf{H}} + D[\hat{\mathbf{S}}_z^2 - S(S+1)/3] + E(\hat{\mathbf{S}}_x^2 - \hat{\mathbf{S}}_y^2) + B_4^0\hat{\mathbf{O}}_4^0 \quad (5)$$

Note that rhombic anisotropy described by the E parameter is permitted by the crystallographic molecular symmetry (C_2). Spectral simulation afforded the following spin-Hamiltonian parameters: $S=6$, $D=-0.179(1)\ \mathrm{cm}^{-1}$, $E=0.018(1)\ \mathrm{cm}^{-1}$, $B_4^0=1.6(5)\times10^{-6}\ \mathrm{cm}^{-1}$, $g_z=1.980(5)$, $g_x=g_y=2.00(1)$, which indicate a predominantly axial magnetic anisotropy ($|E/D|=0.10$). The slight splitting of parallel signals suggests the occurrence of a minority species in the crystal with the same $S=6$, but a smaller D parameter ($-0.170\ \mathrm{cm}^{-1}$). Such a splitting was previously observed in the tetra-iron(III) analogue **Fe_4Ph** as well, and is likely to reflect the disorder of *t*Bu groups or the partial loss of crystallisation Et_2O.[8] The narrow signals observed around H_0 in the spectra at 10 and 20 K could not be reproduced using a giant-spin model, and are likely to reflect transitions within excited states, which become appreciably populated at high temperature (the first excited states lie approximately $21\ \mathrm{cm}^{-1}$ above the ground state). The weak bands visible at 42.1, 50.6, and 59.4 kOe in 230 GHz spectra (10 K) correspond to the typical parallel transitions of tetra-iron(III) complexes. The band positions perfectly match those of a species with $S=5$ and $D=-0.42\ \mathrm{cm}^{-1}$, and thus prove the existence of **Fe_4Ph** in the lattice.[8]

The HF-EPR spectra of **(Ga,Cr)$_4$Ph** recorded at 20, 10, and 5 K with a microwave frequency of 283 GHz are reported in Figure 8. It is evident that on lowering the temperature the partially split perpendicular transition at low field and the parallel one at high field gain intensity. In the strong-field limit this behaviour is readily interpreted as being due to an $S=3/2$ system with $D>0$ and a non-negligible rhombic anisotropy. In this framework, if we assign the above-mentioned lines to the different components of the $|-3/2\rangle\rightarrow|-1/2\rangle$ transition, the difference between (average) perpendicular and parallel resonance fields is $3D/(g\mu_{\mathrm{B}})$, allowing an estimate of $D\approx0.46\ \mathrm{cm}^{-1}$, within the range expected for the axial zfs parameter in octahedral chromium(III) complexes.[23a] Furthermore, the splitting of the low-field perpendicular line, which equals $6E/(g\mu_{\mathrm{B}})$ in the strong-field limit,[23b] suggests a rhombic anisotropy $E\approx0.03\ \mathrm{cm}^{-1}$. Starting from these values, accurate simulation of the spectra was obtained on the basis of Hamiltonian [Eq. (5)] and best-fit parameters $D_c=0.470(5)\ \mathrm{cm}^{-1}$, $E_c=0.029(1)\ \mathrm{cm}^{-1}$, $g_{x,y}=1.977(1)$, $g_z=1.981(1)$ (fourth-order parameters are forbidden for $S=3/2$). An evident feature of the spectra is the strong dependence of the linewidth upon

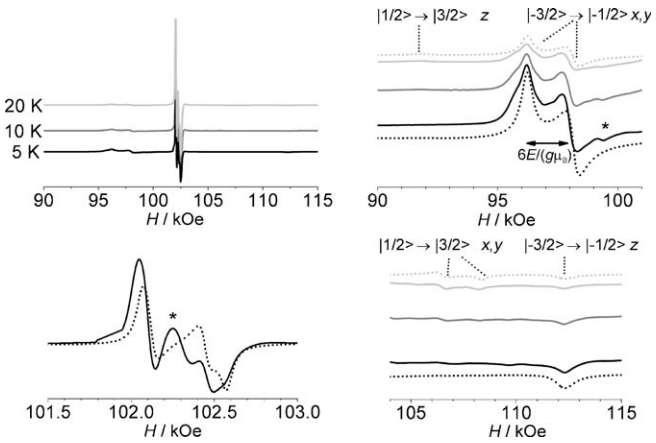

Figure 8. 283 GHz EPR spectra of **(Ga,Cr)$_4$Ph** (solid lines) recorded at 5 K (black), 10 K (dark grey), and 20 K (light grey), along with best-fit simulations (dotted lines, same colour code). Assignment of the transitions is also reported. The asterisks evidence unassigned signals, which we tentatively attribute to a small fraction of chromium(III) ions on the peripheral sites.

the M_S value. The central lines assigned to the $|-1/2\rangle\rightarrow|1/2\rangle$ transition are much sharper than the remaining bands, and a specific and anisotropic linewidth was used for each transition. Our simulation reproduces all observed spectral features, with the exception of very weak additional signals that account for less than 10% of the total spectrum intensity. Within experimental resolution, the chromium(III) ion in **(Ga,Cr)$_4$Ph** is then found to occupy a single site. This implies a chromium-centred structure, in agreement with electronic spectra, or a gallium(III)-centred structure with magnetically equivalent Cr ions in the two crystallographically distinct peripheral sites. The former hypothesis is strongly supported by simple calculations based on the angular overlap model,[24] which show that, for the coordination geometry of the central chromium(III) and setting $Dq=1600\ \mathrm{cm}^{-1}$, a positive zfs of the order of $0.4\ \mathrm{cm}^{-1}$ has to be expected.

The HF-EPR spectra of **(Ga,Fe)$_4$Ph** were recorded between 5 and 20 K at 190 and 230 GHz (see Supporting Information). They were interpreted following the same lines as with the chromium(III)-doped sample: the spectra show the features of an $S=5/2$ system with a positive D (which can be estimated to be about $0.7\ \mathrm{cm}^{-1}$) and a non-negligible rhombic anisotropy (with $E\approx0.08\ \mathrm{cm}^{-1}$). Quite interestingly, these values are very close to those reported by one of us for the iron(III) centres of $[Fe_2(OMe)_2(dbm)_4]$, in which the coordination environment of the metal ions features two *cis*-alkoxide and two β-diketonate ligands, as in the peripheral sites of the tetranuclear complexes studied herein (Hdbm = dibenzoylmethane).[25] A satisfactory simulation of the spectra (see Figure 9) was possible only by assuming the presence of two magnetically inequivalent species (p1 and p2). The observed magnetic inequivalence may be a direct consequence of the two crystallographically distinct peripheral sites, or may be associated with different environments arising from lattice disorder, as observed in **Fe_4Ph**.[8] Because the best simulations were obtained with a 1:1 ratio between

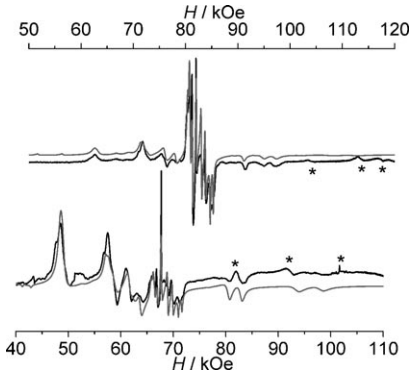

Figure 9. HF-EPR spectra of **(Ga,Fe)$_4$Ph** (black traces) along with best fit simulations (grey traces). Upper spectra: 230 GHz, 20 K; lower spectra: 190 GHz, 5 K. The asterisks mark the transitions resulting from the third harmonics (345 GHz and 285 GHz, respectively) of the fundamental microwave frequencies used in the experiments.

the two species, the former hypothesis implies a preferential occupation of the peripheral site lying on the twofold axis (Fe2 in Figure 2). Single-crystal HF-EPR studies should provide the final answer on this point.

The best agreement with the experimental spectra was obtained with the following parameters: $D_{p1}=0.710(5)$ cm^{-1}, $E_{p1}=0.077(3)$ cm^{-1}; $D_{p2}=0.602(5)$ cm^{-1}, $E_{p2}=0.101(3)$ cm^{-1}. For both centres we set $g_{x,z}=2.001(1)$ and $g_y=2.005(1)$; since the presence of fourth-order parameters, allowed for $S=5/2$, appeared to be unnecessary, an upper limit of $B_4^0=3.0\times10^{-5}$ cm^{-1} was estimated. As in the chromium-doped sample, the peculiar sharpness of the central lines of the spectrum was accounted for by imposing different line widths for resonances characterised by low $|M_S|$ values. The progressive broadening of the EPR bands with increasing $|M_S|$ could explain why the highest-field parallel transitions, expected to lie between 94 and 98 kOe at 190 GHz, are not clearly observed in the experimental spectra. Finally, we notice that occupation of the central site in the structure would result in a trigonally-distorted octahedral geometry for iron(III), which should afford a negative D parameter.[8,26] However, no additional signal attributable to species with negative D is left out by our simulations, thus indicating exclusive substitution on external sites.

It is worth stressing the different location of the paramagnetic dopant in **(Ga,Cr)$_4$Ph** and **(Ga,Fe)$_4$Ph** detected in our spectroscopic studies. In the former, the expected inertness of the $[Cr(L)_2]^{3-}$ unit may favour the formation of a chromium-centred structure, as noted for **Fe$_3$CrPh**. The preference of the iron(III) ions for peripheral sites in **(Ga,Fe)$_4$Ph** is more intriguing, but it is likely to have a thermodynamic rather than kinetic origin.

Alternating current magnetic studies: The significant reduction of the axial anisotropy in **Fe$_3$CrPh** as compared with **Fe$_4$Ph** suggests that the potential energy barrier hampering the reversal of the magnetisation is also reduced, despite the increase in the S value. Assuming in a first approximation that the barrier U is given by $|D|S^2$, from the HF-EPR data we evaluate $U/k_B=9.3$ and 15.0 K for the two species, respectively.[1a] The alternating current (ac) susceptibility of **Fe$_3$CrPh** measured in zero static field reveals a frequency-dependent out-of-phase signal below 5 K, as shown in Figure 10 (the temperature dependence of both in-phase and out-of-phase susceptibilities is reported in the Supporting Information). A complex behaviour with two components is clearly evident, with a minority species relaxing at significantly lower rates. This behaviour is consistent with the occurrence of both chromium-centred Fe_3Cr and Fe_4 complexes in the lattice. The χ'' versus frequency curves suggest that the maximum for the faster relaxing species occurs above the maximum frequency (25 kHz) achievable in our setup. Therefore, we repeated the measurement in an applied field of 1.5 kOe to suppress the zero-field quantum tunnelling and slow down the relaxation. The data, reported in the inset of Figure 10 in the form χ'' versus χ', otherwise known as an Argand plot,[27a] clearly show the presence of two semicircles, underpinning the different dynamics of the two species. The presence of well-defined maxima in χ'', at least for the three lowest temperatures investigated, allowed a semiquantitative analysis based on the generalised Debye model, which includes an empirical parameter α to take into account the width of the distribution of relaxation times.[27b] The χ'' versus frequency data at each temperature were fitted using five adjustable parameters: α (assumed to be the same for the two species), the difference between the isothermal and adiabatic susceptiblities, $\chi_T-\chi_S$, and the relaxation time, τ, for each species (see Supporting Information for more details on the fitting procedure). From the value of $\chi_T-\chi_S$ and the Curie constants for the $S=6$ and $S=5$ states, we estimated a 70:30 ratio between chromium-centred Fe_3Cr and Fe_4 complexes. The amount of Fe_4 is about twice as large as that resulting from static magnetic data. However, given the number of parameters required to simulate the out-of-phase susceptibility, our analysis can be expected to provide only semiquantitative information. The

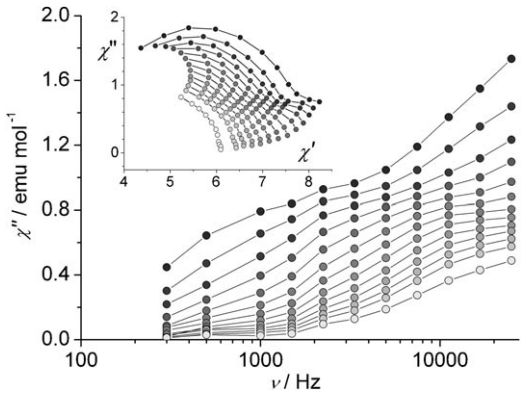

Figure 10. Frequency dependence of the out-of-phase ac susceptibility of **Fe$_3$CrPh** measured in zero static field. The grey scale goes from 1.7 K (dark) to 3.0 K (light). In the inset, the Argand plot obtained in a static field of 1.5 kOe (same colour scale).

same arguments apply to explain the large incertitude associated with relaxation times for the majority species, and, consequently, with the activation parameters obtained by fitting τ versus T data with the Arrhenius law: $\tau_0 = 2.5(6) \times 10^{-7}$ s and $U_{eff}/k_B = 7.0(5)$ K (see Supporting Information). Although measurements at lower temperature and/or higher frequency would be required to evaluate τ_0 and U_{eff} more precisely, the effective barrier in **Fe_3CrPh** is definitely smaller than in **Fe_4Ph** (15.6 K), in agreement with the markedly different spectroscopic barriers of the two compounds (U/k_B=9.3 vs. 15.0 K). In addition, the ground spin state of **Fe_3CrPh** has a larger rhombicity, which is known to accelerate the spin dynamics by promoting quantum tunnelling effects.[1a] The zfs parameter E is indeed comparable in the two compounds, being 0.018 cm^{-1} in **Fe_3CrPh** and 0.023 cm^{-1} in **Fe_4Ph**. However, due to the much lower $|D|$, the $|E/D|$ ratio undergoes an almost twofold increase (from 0.055 to 0.10) upon insertion of chromium(III).

The origin of magnetic anisotropy: The most striking difference observed when comparing the magnetism of **Fe_4Ph** and **Fe_3CrPh** is the increase of the ground spin state from $S=5$ to $S=6$ with concomitant decrease of the D parameter, which varies from -0.418 to -0.179 cm^{-1} upon insertion of chromium(III) as the central metal. The successful synthesis of Cr- and Fe-doped gallium(III) analogues provided a unique opportunity to ascertain the origin of magnetic anisotropy in **Fe_3CrPh** and in the structurally related tetrairon(III) complexes. In order to do this, we used a simplified model taking into account single-ion anisotropies and dipolar interactions only. The anisotropy tensor in the ground spin state (**D**) was expressed as a linear combination of single-ion anisotropies ($\mathbf{D}_i$) and dipolar contributions ($\mathbf{D}_{ij}$), with coefficients calculated in the strong-exchange approximation, as given in Equation (6).[28a]

$$\mathbf{D} = 0.13878(\mathbf{D}_2 + \mathbf{D}_3 + \mathbf{D}_{3'}) + 0.028571\,\mathbf{D}_1 + 0.17347(\mathbf{D}_{23} + \mathbf{D}_{23'} + \mathbf{D}_{33'}) - 0.080952(\mathbf{D}_{12} + \mathbf{D}_{13} + \mathbf{D}_{13'}) = \mathbf{D}^{si} + \mathbf{D}^{dip} \quad (6)$$

When idealised threefold symmetry is assumed, $\mathbf{D}_2$, $\mathbf{D}_3$, and $\mathbf{D}_{3'}$ (and similarly $\mathbf{D}_{23}$, $\mathbf{D}_{23'}$, and $\mathbf{D}_{33'}$ as well as $\mathbf{D}_{12}$, $\mathbf{D}_{13}$, and $\mathbf{D}_{13'}$) are symmetry related. The above tensorial relationship then translates into the following scalar relationship, which involves the anisotropy parameters of peripheral ions (D_p, E_p), the axial zfs of the central ion (D_c), and the dipolar contribution D^{dip}, as given in Equation (7) (a similar formula, but with different projection coefficients, holds for the $S=5$ ground state of **Fe_4Ph**, see references [8,10]).

$$D = 0.20817[D_p(3\cos^2\beta' - 1) + 3\,E_p \sin^2\beta' \cos 2\gamma'] + 0.028571 D_c + D^{dip} \quad (7)$$

The Eulerian angles α', β', and γ' define the orientation of the principal axes (xyz) of $\mathbf{D}_2$ in the molecular frame XYZ, in which Z is the threefold molecular axis and Y is taken along the line joining centres 1 and 2 (see Figure 11). According to the adopted definition of Eulerian angles,[28b] the local frame xyz is obtained from XYZ by three consecutive rotations: around Z by an angle γ', around Y by an angle β', and again around Z by an angle α'. Notice that because Z is a threefold axis, tensors $\mathbf{D}_3$ and $\mathbf{D}_{3'}$ have the same β' and γ' values as $\mathbf{D}_2$, but their α' angles differ by 120° and 240°, respectively (α' has no influence on D). A dipolar anisotropy $D^{dip} = -0.0132$ cm^{-1} was estimated in the point-dipolar approximation by setting an isotropic $g=2.00$ and using the known intermetal separations.[28a] It has to be noted that the shorter metal-to-metal distances in **Fe_3CrPh** lead to stronger pairwise dipolar interaction compared with **Fe_4Ph**. However,

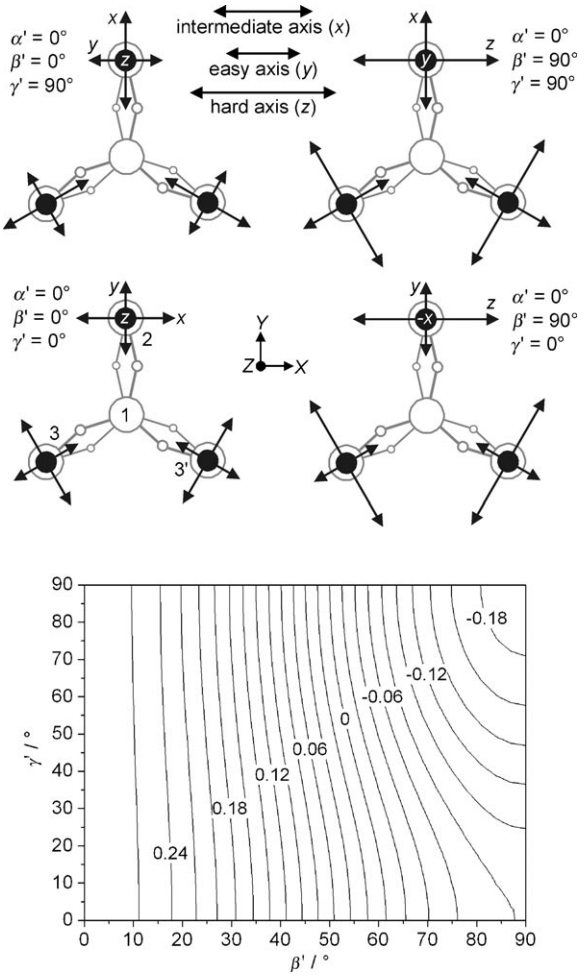

Figure 11. Upper panel: Representative arrangements of anisotropy tensors for the peripheral iron(III) ions in **Fe_3CrPh** assuming threefold molecular symmetry. The Eulerian angles α', β', and γ' define the orientation of the principal anisotropy axes (xyz) of centre 2 in the molecular frame XYZ (see text). As a simultaneous rotation of all tensors around Z does not affect the D parameter, the α' angle is set to 0° for simplicity (i.e., z is kept in the XZ plane; for a justification see references [8,10]). Lower panel: Contour plot showing the D parameter (in cm^{-1}) calculated from Equation (7) as a function of β' and γ'. The graph is symmetric around $\beta'=0$, $\beta'=90°$, $\gamma'=0$ and $\gamma'=90°$. Contour levels are shown at 0.02 cm^{-1} intervals. The observed D value is reproduced with $\beta'=\gamma'=90°$, that is, by orienting the local easy axis (y) along Z, as in the top right diagram of the upper panel.

the dipolar contribution in this compound is considerably reduced with respect to **Fe_4Ph** ($D^{dip} = -0.0367\ cm^{-1}$) due to the smaller projection coefficients. In both cases, the point-dipolar terms account for less than 10% of the observed anisotropy, which is therefore dominated by single-ion contributions. Considering that **Ga_4Ph** is isomorphous with **Fe_3CrPh**, the Cr- and Fe-doped compounds have been used to gain accurate information on the electronic structure of the metal ions in **Fe_3CrPh**. By setting $D_c = 0.470\ cm^{-1}$ in Equation (7), the calculated contribution of the chromium(III) ion to D is $+0.0134\ cm^{-1}$ and almost exactly cancels out the dipolar term. Therefore, the negative sign of D and, consequently, the observed SMM behaviour, depend crucially on the anisotropy of the peripheral metal centres. Using average zfs parameters $D_p = (D_{p1} + D_{p2})/2 = 0.656\ cm^{-1}$ and $E_p = (E_{p1} + E_{p2})/2 = 0.089\ cm^{-1}$, Equation (7) can be applied to calculate the expected D value as a function of β' and γ'. The results, reported in Figure 11 as a contour plot, clearly indicate that in order to reproduce the observed D value both β' and γ' need to be close to 90°. Hence, the hard axes (z) of the peripheral ions must lie approximately in the molecular plane, and the local "easy" directions (y) must be aligned roughly along Z so as to project a large negative zfs component along the same axis.

The observation that all metal ions in **Fe_3CrPh** have a substantial hard-axis anisotropy demonstrates that SMM behaviour may well arise from magnetic units with $D > 0$, provided that the single-ion tensors are suitably oriented with respect to each other. A related mechanism was shown by Kajiwara, Nakano and co-workers to be operative in a single-chain magnet.[29] As the structures of **Fe_3CrPh** and **Fe_4Ph** are very similar, it is likely that the magnetic anisotropy in the latter can be correctly interpreted in a similar fashion, as previously suggested to explain magnetostructural correlations in the family of tetra-iron(III) propellers.[8,10] It has to be noticed that the enhanced $|D|$ parameter found in the Fe_4 species originates both from the larger coefficient appearing in the corresponding projection formulae and from the extra, easy-axis-type contribution expected for the central ion.[8,26]

Conclusion

The iron(III)–chromium(III) single molecule magnet (SMM) $[Fe_3Cr(L)_2(dpm)_6]\cdot Et_2O$ (**Fe_3CrPh**), featuring a chromium-centred triangular topology of metal ions, has an $S = 6$ ground state and an easy-axis magnetic anisotropy with $D = -0.179(1)\ cm^{-1}$. Slow relaxation of the magnetisation is observed, although with a lower energy barrier than for the homometallic derivative **Fe_4Ph** ($U_{eff}/k_B = 7.0$ K vs. 15.6 K). According to detailed spectroscopic studies on a doped tetragallium(III) analogue, the Cr^{3+} and Fe^{3+} ions in **Fe_3CrPh** have hard-axis anisotropies, with D parameters in the range 0.5–0.7 cm^{-1}. Interestingly, the anisotropic contributions provided by the central chromium(III) ion and by point dipolar interactions cancel out almost exactly. The observed molecular anisotropy is thus ruled by the peripheral iron(III) ions, and can be reproduced by setting their hard axes approximately perpendicular to the idealised threefold molecular axis. Fully confirming previous arguments,[8,10] the SMM properties of **Fe_4Ph** and of other tetra-iron(III) complexes currently investigated in the field of molecular spintronics are also likely to arise from a similar mechanism, with an extra easy-axis contribution from the central iron(III) ion.

The proposed treatment neglects other sources of magnetic anisotropy, such as anisotropic exchange or Dzyaloshinkii–Moriya interactions, the impact of which on SMM behaviour is still under debate.[25,28a,30] Nevertheless, our findings demonstrate that SMM properties can be observed in systems comprising hard-axis metal ions only. Taking into proper account the non-collinearity of single-ion anisotropy tensors may thus be essential not only to understand magnetic quantum tunnelling effects,[31] but also to explain the most canonical feature of SMMs, that is, their anisotropy barrier.

Experimental Section

General: Proton NMR spectra were recorded on a Bruker FT-DPX200 NMR spectrometer. 2-Hydroxymethyl-2-phenylpropane-1,3-diol (H_3L),[32] $[Fe_2(OMe)_2(dpm)_4]$ (**Fe_2**),[8] $[Cr_2(OMe)_2(dpm)_4]$ (**Cr_2**)[15] and $CrCl_3(THF)_3$[11] were prepared by literature methods. Diethyl ether (from a freshly opened can, pre-dried over $CaCl_2$ overnight) and toluene were distilled from Na/benzophenone before use. Methanol was carefully dried by treatment with Mg/I_2 and distilled prior to use. Sodium methoxide (≈3 M in methanol) was prepared by careful addition of sodium metal to anhydrous methanol under nitrogen. The $GaCl_3$ stock solution (0.01344 M in MeOH) was prepared by cautious addition of $GaCl_3$ to anhydrous MeOH under nitrogen (*ATTENTION: violent reaction!*). Elemental analysis was carried out on a CE Instruments EA1110 analyser. Fe and Cr contents were measured by complexometric titration with EDTA, following the kinetic masking technique.[12] ESI mass spectra were obtained with an ESI Waters ZQ-4000 instrument. The synthesis of the complexes did not require an inert atmosphere, though precautions were taken to avoid prolonged contact with atmospheric moisture.

Synthesis of $[Fe_3Cr(OMe)_6(dpm)_6]$ (Fe_3Cr): $[CrCl_3(thf)_3]$ (55.4 mg, 0.148 mmol) was added to a suspension of **Fe_2** (201.5 mg, 0.2222 mmol) in 1:2 (v/v) methanol:diethyl ether (19 mL), and the mixture was stirred until it turned into a clear deep red solution. NaOMe (3.081 M in methanol, 0.15 mL, 0.46 mmol) was introduced dropwise with vigorous stirring, and stirring was continued for 20 min (during this period, a red–brown precipitate formed). A 1:4 (v/v) methanol:diethyl ether mixture (62 mL) was then added to the suspension, which was stirred for 15 min and left undisturbed overnight. The solid was removed by filtration on a G4 frit, and the solution was divided into two 40 mL portions. Slow diffusion of methanol vapours (80 mL) in one of the two portions over two weeks afforded reddish-brown rod-like crystals, which were collected by filtration, washed with the external diffusion mixture, and dried under vacuum (88.6 mg, 80%). ESI-MS (2.1 mM, toluene): $m/z = 628$ $[Fe(dpm)_3+Na]^+$; elemental analysis calcd (%) for $Fe_3CrO_{18}C_{72}H_{132}$: C 57.45, H 8.84, Fe 11.13, Cr, 3.45; found: C 57.80, H 9.60, Fe 12.22, Cr 2.75 (Fe:Cr = 4.14 mol/mol).

Synthesis of $[Fe_3Cr(L)_2(dpm)_6]\cdot Et_2O$ (Fe_3CrPh): The remaining 40 mL portion of the filtered reaction mixture was treated with solid H_3L (38.2 mg, 0.21 mmol), and the suspension was stirred until complete dissolution of the ligand (10 min). Slow diffusion of methanol vapours (80 mL) over two weeks afforded long red–black rods, which were col-

lected by filtration, washed with the external diffusion mixture, and dried under mild vacuum (400 mm Hg, 5 min) to avoid loss of lattice solvent (70.2 mg, 54%). ESI-MS (2.1 mM, toluene): $m/z = 1701$ $[M+Na]^+$, 1677 $[M]^+$, 1493 $[M-dpm]^+$, 628 $[Fe(dpm)_3+Na]^+$; elemental analysis calcd (%) for $Fe_3CrO_{19}C_{90}H_{146}$: C 61.71, H 8.40, Fe 9.56, Cr 2.97; found: C 61.30, H 8.78, Fe 10.14, Cr 2.51 (Fe:Cr = 3.76 mol/mol).

Synthesis of $[Ga_2(OMe)_2(dpm)_4]$ (Ga_2): $GaCl_3$ (0.359 g, 2.04 mmol) was cautiously dissolved in MeOH (20 mL) under nitrogen (*ATTENTION: violent reaction!*). Dropwise addition of a solution of Hdpm (0.752 g, 4.08 mmol) and NaOMe (3.081 M in methanol, 2.45 mL, 7.55 mmol) in MeOH (10 mL) under stirring resulted in precipitation of a white solid, which was stirred overnight, collected by filtration over a G3 frit, washed copiously with MeOH, and finally dried in vacuum (0.611 g, 64%). The product was used for the subsequent reaction step without further purification.

Synthesis of $[Ga_4(L)_2(dpm)_6]\cdot Et_2O$ (Ga_4Ph): The Ga_2 dimer prepared as above (0.192 g, 0.205 mmol) was suspended in Et_2O (14.5 mL). $GaCl_3$ (0.01344 M in MeOH, 10.2 mL, 0.137 mmol) was added with stirring. After 30 min of stirring a clear colourless solution was obtained, to which NaOMe (3.047 M in methanol, 0.14 mL, 0.43 mmol) was added with thorough stirring. The resulting colourless suspension was stirred for 10 min, Et_2O (50 mL) and H_3L (80 mg, 0.44 mmol) were added, and the mixture was stirred and left undisturbed overnight. The precipitated NaCl was filtered off using a G4 frit. Slow vapour diffusion of MeOH (100 mL) into the clear solution afforded rod-like, off-white crystals of the desired product, which were washed with MeOH and quickly dried in vacuum (204 mg, 82%). ^{1}H NMR (200 MHz, [D$_6$]benzene, 30°C, TMS): $\delta = 1.14$ (s, 54H; *t*Bu), 1.36 (s, 54H; *t*Bu), 4.97 (d, $^2J(H,H) = 9.7$ Hz, 6H; CH_2O), 5.50 (d, $^2J(H,H) = 9.7$ Hz, 6H; CH_2O), 5.73 (s, 6H; =CH−), 6.90 (t, $^3J(H,H) = 7.5$ Hz, 2H; *p*-Ph), 7.18 (t, $^3J(H,H) = 7.5$ Hz, 4H; *m*-Ph), 7.69 ppm (d, $^3J(H,H) = 7.5$ Hz, 4H; *o*-Ph); elemental analysis calcd (%) for $Ga_4O_{19}C_{90}H_{146}$: C 59.69, H 8.13; found: C 60.01, H 8.40.

Synthesis of $[Ga_{3.75}Fe_{0.25}(L)_2(dpm)_6]\cdot Et_2O$ ($(Ga,Fe)_4Ph$): The Ga_2 dimer prepared as above (0.207 g, 0.222 mmol) was suspended in Et_2O (12 mL). $GaCl_3$ (0.01344 M in MeOH, 8.26 mL, 0.111 mmol) and then solid $FeCl_3$ (6.0 mg, 0.037 mmol) were added in sequence with stirring. After 10 min of stirring a clear, orange solution was obtained, to which NaOMe (3.081 M in methanol, 0.15 mL, 0.46 mmol) was added with thorough stirring. The resulting yellow suspension was stirred for 15 min, Et_2O (50 mL) and H_3L (80 mg, 0.44 mmol) were added, and the mixture was stirred overnight. The precipitated NaCl was filtered off using a G4 frit. Slow vapour diffusion of MeOH (100 mL) into the clear yellow solution afforded rod-like, yellow crystals of the desired product, which were washed with MeOH and quickly dried in vacuum (186 mg, 69%). XRD analysis showed the crystals to be isomorphous with those of Ga_4Ph ($T = 298$ K; $a = 19.59(1)$, $b = 22.14(1)$, $c = 24.60(2)$ Å; $\beta = 107.83(2)°$; $V_c = 10157(8)$ Å^3; monoclinic *C*).

Synthesis of $[Ga_{3.75}Cr_{0.25}(L)_2(dpm)_6]\cdot Et_2O$ ($(Ga,Cr)_4Ph$): The preparation is similar to that previously described, replacing $FeCl_3$ with $[CrCl_3(thf)_3]$ (14.3 mg, 0.038 mmol). The reaction mixture has a bottle-green colour, but turns progressively to blue upon vapour diffusion of MeOH. The rod-like crystals of the product are bright blue and dichroic (violet to blue) (185 mg, 69%). XRD analysis showed the crystals to be isomorphous with those of Ga_4Ph ($T = 298$ K; $a = 19.59(2)$, $b = 22.15(2)$, $c = 24.63(2)$ Å; $\beta = 107.89(2)°$; $V_c = 10167(10)$ Å^3, monoclinic *C*).

X-ray crystallography: Single-crystal X-ray diffraction investigations on Fe_3Cr, Fe_3CrPh and Ga_4Ph were carried out using a four-circle Bruker X8-APEX diffractometer equipped with $Mo_{K\alpha}$ generator, area detector, and Kryo-Flex cryostat. Evaluation of the crystal quality and determination of unit cell parameters were based on 60 preliminary frames collected using ω scans. Structure solution and refinement were successfully carried out in the centrosymmetric space group *C*2/*c*, as in homometallic derivatives, using SIR92[33a] and SHELXL-97[33b] software implemented in WINGX.[33c] Details of the X-ray analysis of Fe_3Cr and Ga_4Ph are given in the Supporting Information, and we herein focus on Fe_3CrPh only. Disorder effects were limited to a *t*Bu group of a dpm ligand coordinated to Fe3, and were modelled over two positions with 0.74 and 0.26 occupancies. All non-hydrogen atoms were refined anisotropically, and hydrogen atoms were set in idealised positions and assigned isotropic displacement parameters 50% and 20% larger than the attached carbon atom for CH_3 and CH_2/CH groups, respectively.

CCDC-772027 (Fe_3CrPh), 772028 (Ga_4Ph) and 773871 (Fe_3Cr) contain the supplementary crystallographic data for this paper. These data can be obtained free of charge from The Cambridge Crystallographic Data Centre via www.ccdc.cam.ac.uk/data_request/cif.

Electronic spectra: UV/Vis spectra in toluene were recorded on a Perkin–Elmer Lambda 650 spectrometer using either 1, 0.5, or 0.1 cm optical paths. The contribution of the solvent was subtracted in all the spectral range, and the measured absorbances were converted to molar absorption coefficients using the Lambert–Beer law.

Magnetic measurements: Direct current magnetic measurements on 7.72 and 5.04 mg samples of Fe_3CrPh and Fe_3Cr were made using a Quantum Design MPMS SQUID magnetometer with applied fields of 10 kOe (for $T > 30$ K) and 1 kOe (for $T \leq 30$ K). Raw susceptibility data were reduced with molecular weights of 1751.62 and 1505.33, and diamagnetic correction of -1028.2×10^{-6} and -871.3×10^{-6} emu mol^{-1}, corresponding to the formulas $[Fe_3Cr(L)_2(dpm)_6]\cdot Et_2O$ and $[Fe_3Cr(OMe)_6(dpm)_6]$, respectively. Magnetisation isotherms in fields up to 50 kOe were recorded at three different temperatures (1.9, 2.5, and 4.5 K). The alternating current magnetic susceptibility of the same Fe_3CrPh sample was measured with a home-made induction probe adapted to work in an Oxford Instruments MAG2000 platform.

HF-EPR spectra: HF-EPR experiments were carried out at Laboratoire National des Champs Magnétiques Intenses-CNRS (Grenoble, France) using a home-made spectrometer equipped with a continuous-flow cryostat, two Gunn diodes operating at 95 and 115 GHz, and a second-harmonic generator to produce the frequencies of interest (190 and 230 GHz). The second harmonic generator also produces a small contribution of third harmonics (285 and 345 GHz, respectively). The frequency of 283.2 GHz was obtained using a triple harmonic generator after a 94.4 GHz initial frequency supplied by an actively multiplied dielectric resonator oscillator (DRO). The spectra were recorded at 5, 10, and 20 K in fields up to 120 kOe on microcrystalline samples ground using a pestle and mortar and pressed into a pellet to avoid field-induced preferential orientation of the crystallites.

Spin Hamiltonian calculations: The fitting of direct current magnetic data and the calculation of local spin polarisation were performed using software developed in-house.[17] Simulations of HF-EPR spectra were obtained by diagonalisation of the full spin-Hamiltonian matrix using dedicated software.[22a,b]

Acknowledgements

The work was financed by NE MAGMANET (FP6-NMP3-CT-2005-515767), and the ERANET project "NanoSci-ERA: NanoScience in the European Research Area" (SMMTRANS), as well as by Italian PRIN and FIRB grants. We gratefully acknowledge Luca Zuppiroli (Department of Organic Chemistry, Faculty of Industrial Chemistry, University of Bologna, Italy) for ESI-MS experiments. We thank A. B. P. Lever (York University, Canada) for stimulating discussion on electronic spectra.

[1] a) D. Gatteschi, R. Sessoli, J. Villain, *Molecular Nanomagnets*, Oxford University Press, Oxford, **2006**; b) C. J. Milios, A. Vinslava, W. Wernsdorfer, S. Moggach, S. Parsons, S. P. Perlepes, G. Christou, E. K. Brechin, *J. Am. Chem. Soc.* **2007**, *129*, 2754–2755; c) C. J. Milios, R. Inglis, A. Vinslava, R. Bagai, W. Wernsdorfer, S. Parsons, S. P. Perlepes, G. Christou, E. K. Brechin, *J. Am. Chem. Soc.* **2007**, *129*, 12505–12511.

[2] A. Cornia, A. Fabretti Costantino, L. Zobbi, A. Caneschi, D. Gatteschi, M. Mannini, R. Sessoli, *Struct. Bonding* **2006**, *122*, 133–161.

[3] a) L. Bogani, W. Wernsdorfer, *Nat. Mater.* **2008**, *7*, 179 –186; b) D. Gatteschi, A. Cornia, M. Mannini, R. Sessoli, *Inorg. Chem.* **2009**, *48*, 3408–3419; c) A. R. Rocha, V. M. García-Suárez, S. W. Bailey, C. J. Lambert, J. Ferrer, S. Sanvito, *Nat. Mater.* **2005**, *4*, 335–339; d) M. Misiorny, I. Weymann, J. Barnas, *Europhys. Lett.* **2010**, *89*, 18003.
[4] M. Mannini, F. Pineider, Ph. Sainctavit, C. Danieli, E. Otero, C. Sciancalepore, A. M. Talarico, M.-A. Arrio, A. Cornia, D. Gatteschi, R. Sessoli, *Nat. Mater.* **2009**, *8*, 194–197.
[5] F. Pineider, M. Mannini, C. Danieli, L. Armelao, F. M. Piras, A. Magnani, A. Cornia, R. Sessoli, *J. Mater. Chem.* **2010**, *20*, 187–194.
[6] L. Margheriti, M. Mannini, L. Sorace, L. Gorini, D. Gatteschi, A. Caneschi, D. Chiappe, R. Moroni, F. Buatier de Mongeot, A. Cornia, F. M. Piras, A. Magnani, R. Sessoli, *Small* **2009**, *5*, 1460–1466.
[7] R. W. Saalfrank, I. Bernt, M. M. Chowdhry, F. Hampel, G. B. M. Vaughan, *Chem. Eur. J.* **2001**, *7*, 2765–2769.
[8] S. Accorsi, A.-L. Barra, A. Caneschi, G. Chastanet, A. Cornia, A. C. Fabretti, D. Gatteschi, C. Mortalò, E. Olivieri, F. Parenti, P. Rosa, R. Sessoli, L. Sorace, W. Wernsdorfer, L. Zobbi, *J. Am. Chem. Soc.* **2006**, *128*, 4742–4755.
[9] G. G. Condorelli, A. Motta, G. Pellegrino, A. Cornia, L. Gorini, I. L. Fragalà, C. Sangregorio, L. Sorace, *Chem. Mater.* **2008**, *20*, 2405–2411.
[10] L. Gregoli, C. Danieli, A.-L. Barra, P. Neugebauer, G. Pellegrino, G. Poneti, R. Sessoli, A. Cornia, *Chem. Eur. J.* **2009**, *15*, 6456–6467.
[11] W. Herwig, H. H. Zeiss, *J. Org. Chem.* **1958**, *23*, 1404.
[12] J. H. Jeffery, J. Bassett, J. Mendham, R. C. Denney, *Vogel Analisi Chimica Quantitativa*, Casa Editrice Ambrosiana, Milano, **1995**, p. 378.
[13] The Fe/Cr ratio was found to vary slightly in different preparations based on the same procedure. Use of excess $[CrCl_3(thf)_3]$ in the synthesis did not increase the chromium(III) content in the product.
[14] F. Le Gall, F. Fabrizi de Biani, A. Caneschi, P. Cinelli, A. Cornia, A. C. Fabretti, D. Gatteschi, *Inorg. Chim. Acta* **1997**, *262*, 123–132.
[15] H. R. Fischer, D. J. Hodgson, E. Pedersen, *Inorg. Chem.* **1984**, *23*, 4755–4758.
[16] R. D. Shannon, C. T. Prewitt, *Acta Crystallogr. Sect. B* **1970**, *26*, 1046–1048.
[17] A.-L. Barra, F. Bianchi, A. Caneschi, A. Cornia, D. Gatteschi, L. Gorini, L. Gregoli, M. Maffini, F. Parenti, R. Sessoli, L. Sorace, A. M. Talarico, *Eur. J. Inorg. Chem.* **2007**, 4145–4152.
[18] a) R. L. Lintvedt, L. K. Kernitsky, *Inorg. Chem.* **1970**, *9*, 491–494; b) A. B. P. Lever, *Inorganic Electron Spectroscopy*, 2nd ed., Elsevier, Amsterdam, **1984**; c) R. Dingle, *J. Chem. Phys.* **1969**, *50*, 1952–1957; d) A. M. Fatta, R. L. Lintvedt, *Inorg. Chem.* **1971**, *10*, 478–481.
[19] A. B. Blake, A. Yavari, W. E. Hatfield, C. N. Sethulekshmi, *J. Chem. Soc. Dalton Trans.* **1985**, 2509–2520.
[20] a) I. Bertini, C. Luchinat, *Coord. Chem. Rev.* **1996**, *150*, 1–296; b) K. Douglas Kissler, S. K. Sheppard, G. R. Eaton, S. S. Eaton, *J. Magn. Reson.* **1985**, *63*, 74–87; c) B. Ballarin, G. A. Battiston, F. Benetollo, R. Gerbasi, M. Porchia, D. Favretto, P. Traldi, *Inorg. Chim. Acta* **1994**, *217*, 71–78.
[21] A. L. Barra, L. C. Brunel, D. Gatteschi, L. Pardi, R. Sessoli, *Acc. Chem. Res.* **1998**, *31*, 460–466.
[22] a) C. J. H. Jacobsen, E. Pedersen, J. Villadsen, H. Weihe, *Inorg. Chem.* **1993**, *32*, 1216–1221; b) S. Mossin, H. Weihe, A.-L. Barra, *J. Am. Chem. Soc.* **2002**, *124*, 8764–8765; c) A. Abragam, B. Bleaney, *Electron Paramagnetic Resonance of Transition Ions*, Dover Publications, New York, **1986**.
[23] a) A. Bencini, D. Gatteschi in *Transition Metal Chemistry, Vol. 8* (Eds.: G. A. Melson, B. N. Figgis), Marcel Dekker, New York, **1982**; b) A. Solano-Peralta, M. E. Sosa-Torres, M. Flores-Alamo, H. El-Mkami, G. M. Smith, R. A. Toscano, T. Nakamura, *Dalton Trans.* **2004**, 2444–2449.
[24] A. Bencini, I. Ciofini, M. G. Uytterhoeven, *Inorg. Chim. Acta* **1998**, *274*, 90–101.
[25] P. ter Heerdt, M. Stefan, E. Goovaerts, A. Caneschi, A. Cornia, *J. Magn. Reson.* **2006**, *179*, 29–37.
[26] a) J. Ribas-Arino, T. Baruah, M. R. Pederson, *J. Chem. Phys.* **2005**, *123*, 044303; b) A. Cornia, A. C. Fabretti, P. Garrisi, C. Mortalò, D. Bonacchi, D. Gatteschi, R. Sessoli, L. Sorace, W. Wernsdorfer, A.-L. Barra, *Angew. Chem.* **2004**, *116*, 1156–1159; *Angew. Chem. Int. Ed.* **2004**, *43*, 1136–1139; c) D. Gatteschi, L. Sorace, *J. Solid State Chem.* **2001**, *159*, 253–261; d) A.-L. Barra, A. Caneschi, A. Cornia, F. Fabrizi de Biani, D. Gatteschi, C. Sangregorio, R. Sessoli, L. Sorace, *J. Am. Chem. Soc.* **1999**, *121*, 5302–5310.
[27] a) C. Dekker, A. F. M. Arts, H. W. Wijn, A. J. van Duyneveldt, J. A. Mydosh, *Phys. Rev. B* **1989**, *40*, 11243–11251; b) K. S. Cole, R. H. Cole, *J. Chem. Phys.* **1941**, *9*, 341–351.
[28] a) A. Bencini, D. Gatteschi, *EPR of Exchange Coupled Systems*, Springer, Berlin, **1990**; b) B. Silver, *Irreducible Tensor Methods—An Introduction for Chemists*, Academic Press, New York, **1976**.
[29] T. Kajiwara, M. Nakano, Y. Kaneko, S. Takaishi, T. Ito, M. Yamashita, A. Igashira-Kamiyama, H. Nojiri, Y. Ono, N. Kojima, *J. Am. Chem. Soc.* **2005**, *127*, 10150–10151.
[30] a) W. Wernsdorfer, T. C. Stamatatos, G. Christou, *Phys. Rev. Lett.* **2008**, *101*, 237204/1–4; b) E. del Barco, S. Hill, D. N. Hendrickson, *Phys. Rev. Lett.* **2009**, *103*, 059701/1; c) W. Wernsdorfer, T. C. Stamatatos, G. Christou, *Phys. Rev. Lett.* **2009**, *103*, 059702/1; d) F. Cinti, M. Affronte, A. G. M. Jansen, *Eur. Phys. J. B* **2002**, *30*, 461–468; e) N. Kirchner, J. Van Slageren, B. Tsukerblat, O. Waldmann, M. Dressel, *Phys. Rev. B* **2008**, *78*, 094426/1–5.
[31] A.-L. Barra, A. Caneschi, A. Cornia, D. Gatteschi, L. Gorini, L.-P. Heiniger, R. Sessoli, L. Sorace, *J. Am. Chem. Soc.* **2007**, *129*, 10754–10762.
[32] R. Viguier, S. Serratrice, A. Dupraz, C. Dupuy, *Eur. J. Inorg. Chem.* **2001**, 1789–1795.
[33] a) A. Altomare, G. Cascarano, C. Giacovazzo, A. Guagliardi, *J. Appl. Crystallogr.* **1993**, *26*, 343–350; b) SHELX97, Programs for Crystal Structure Analysis, G. M. Sheldrick, University of Göttingen, Göttingen, **1997**; c) L. J. Farrugia, *J. Appl. Crystallogr.* **1999**, *32*, 837–838.

Received: April 20, 2010
Published online: July 23, 2010

